

**Reactive Robot Control and Sensing Systems**

by

**Caleb Sebastian Escobedo**

B.S., Trinity University, 2019

An area exam submitted to the  
Faculty of the Graduate School of the  
University of Colorado in partial fulfillment  
of the requirements for the degree of  
Doctor of Philosophy  
Department of Computer Science  
2023

This area exam entitled:  
Reactive Robot Control and Sensing Systems  
written by Caleb Sebastian Escobedo  
has been approved for the Department of Computer Science

---

Dr. Alessandro Roncone

---

Dr. Christoffer Heckman

---

Dr. Ibrahim Volkan Isler

Date \_\_\_\_\_

Escobedo, Caleb Sebastian (Ph.D., Computer Science)

Reactive Robot Control and Sensing Systems

Area exam directed by Dr. Alessandro Roncone

## Contents

### Chapter

<b>1</b>	Introduction	<b>1</b>
<b>2</b>	Onboard Sensors	<b>5</b>
2.1	BioTac . . . . .	5
2.2	Optical-Tactile Sensors . . . . .	6
2.3	Capacitive . . . . .	8
2.4	Hexagonal Array . . . . .	8
2.5	Acoustic . . . . .	10
<b>3</b>	Control with Sensing Feedback	<b>12</b>
<b>4</b>	Control	<b>16</b>
4.1	Quadratic Programming Optimization . . . . .	17
4.1.1	Explicit Reference Governor . . . . .	18
4.2	Non-Linear Optimization . . . . .	20
<b>5</b>	Conclusions	<b>23</b>
	<b>Bibliography</b>	<b>25</b>

## Figures

## Figure

3.1	Top shows an example human collision detection using only proprioceptive sensors, adapted from [3]. Bottom shows a seven event collision detection pipeline, presented in [22]. . . . .	13
3.2	Left shows the proximity signal detection and robot stopping pipeline form [15]. Right shows stiffness adjustment and path deviation to reduce collision force ,from [5].	14
3.3	Top shows the iCub robot with taxel sensors along its body. These are used along with its vision system to estimate where objects near the body are most likely to make contact [38]. Bottom shows an adapted visual reactive preshaping example using proximity sensors for the robot gripper to adjust a grab approach prior to making contact [34]. . . . .	15
3.4	Top shows capacative sensor array used for autonomous human dressing and washing tasks. Bottom shows the coordinate axes and variables used to formally define the end-effector position relative to a human limb. Images adapted from [13]. . . . .	15
4.1	Top left shows the repulsive vectors to a control point, such as the end-effector, when the object velocity is included or excluded. Bottom left shows how object distances are calculated with occlusions from the camera's point of view. Right shows the raw depth data on the screen while a human approaches the robot, triggering avoidance behavior. Figures are from [18]. . . . .	17
4.2	Top shows obstacle avoidance while the robot end-effector moves between two points. Bottom left shows a common quadratic programming formulation for objective functions with constraints. Bottom right illustrates how movement restrictions are placed along the robot body for multiple objects. The colored spheres are the acceptable velocities for each of the points that can move. Figures are from [4]. . . . .	18

4.3 Top image shows the robot end-effector's angular velocity manipulability ellipsoid in two configurations, from [23]. Bottom left image shows the object avoidance calculation distance with a minimum avoidance distance around the object. Bottom right shows an example scenario where a robot avoids a collision and achieves a goal position. Bottom images are from [24]. . . . .	19
4.4 Top diagram shows the control blocks for the ERG based collision avoidance controller. Bottom left shows an example dynamic safety margin prediction and actual joint positions over time. Bottom right shows a real-world avoidance example using vicon markers for sensing the human subject. All figures are from [31]. . . . .	20
4.5 Objective normalization function of a gaussian surrounded by a polynomial, from [36].	21
4.6 Point cloud to convex hull representation for collision avoidance objective functions [37]. . . . .	22
4.7 The left image shows example robot arm objective function types: Red – specific goal, Green – range of equally valid goals, and Blue – range of goal with a preference toward certain values. These correspond to the Groove, Swamp, and Swamp Groove graphs, respectively. These figures were adapted from [43]. . . . .	22

## **Chapter 1**

### **Introduction**

Sensors have increasingly become embedded into devices that humans interact with on a daily basis, resulting in enhanced expressiveness and safety. This advancement in sensing technology has revolutionized the transfer of information between humans and their devices. A prime example of improved sensing is the incorporation of touch screens in phones, complemented by vibration feedback. These haptic sensations simulate the tactile experience of pressing physical buttons, making interactions more intuitive and expressive. Additionally, the widespread adoption of car backup cameras with audio distance signals has greatly improved safety while reversing, and are now standard in cars. As the amount of time spent with devices and the complexity of conveyed information has continued to increase, monitoring systems have become commonplace in semi-autonomous vehicles. These systems monitor driver alertness and enforce periodic manual intervention, thereby ensuring heightened safety on the road. According to a white paper by TE Automotive in 2016, it was estimated that, at that time, most cars are equipped with approximately 60 to 100 sensors. The paper also projected that the number of sensors in cars is expected to double within a 10-year timeframe [12].

Furthermore, smart watches equipped with biometric sensors analyze vital data to encourage healthy habits such as regular physical activity, adequate sleep, and stress monitoring. Access to sensors has increased due to their common use in commercially available products such as cars, phones, homes, and watches. The trend in the cost of Internet of Things (IoT) sensors, commonly used in households for detecting external stimuli in 2019, is depicted in fig. 1.1. With increased

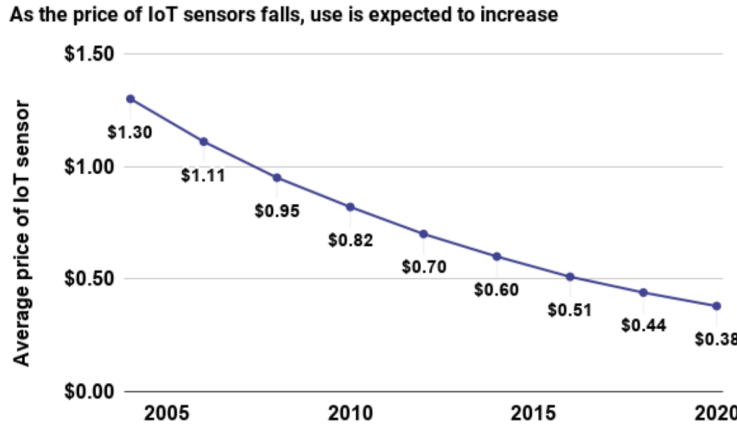


Figure 1.1: Graph shows the trend in cost of Internet of Things, sensors taken from [29]

availability and cost reduction through mass production, sensors are now being adapted for use in various fields. Specifically, robot arms can take advantage of precise and fast sensor data in real-time. This integration holds great potential for enhancing expressiveness and enabling smooth collaboration in physical human-robot interaction systems.

Current collaborative robot (cobot) systems rely on two main sensing techniques for trajectory planning and control execution. The first is vision, which typically involves RGB or depth systems. The second is force/torque sensors integrated into the robot's motors. However, these systems have limitations, particularly in dynamic environments with physical interactions. Robots equipped with vision systems often face challenges such as occlusions, as depicted in fig. 1.2. These occlusions hinder the robot's ability to accurately perceive the environment, including determining the 3D object volume, movement direction, and properties relevant to the intended physical manipulation [34]. Additionally, vision systems require computationally expensive computer vision processing, which can introduce delays and impact real-time control.

One of the major hurdles in equipping and processing additional sensor information for robot manipulators lies in identifying and formulating the appropriate robot behavior in response to sensor stimuli. While close-proximity ( $< 15$  cm) sensors are commonly used for collision avoidance, simply avoiding a collision does not foster interactive behavior, and each situation may require a

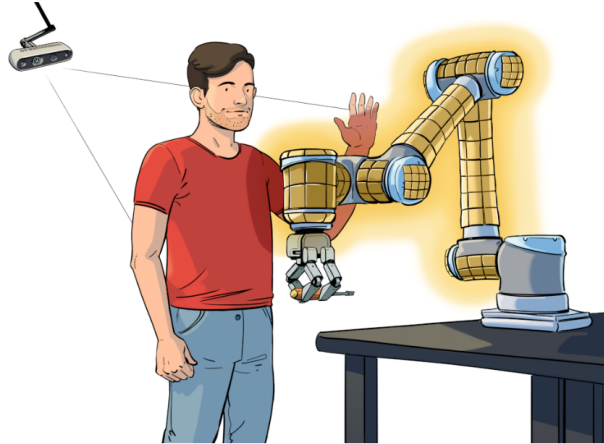


Figure 1.2: Human-Robot interaction scenario from [34], where the externally mounted camera shown in the top left is not able to accurately perceive the environment due to the human blocking its view. Onboard proximity sensors are shown on the robot with a yellow aura, depicting the detectable area.

unique interactive response from the robot [34]. Additionally, predefined reactions based on nearby objects do not necessarily focus on enhancing human-robot interaction.

To promote effective and intuitive collaboration, robots should possess the ability to intelligently adjust their method of interaction in subtle ways. This means enabling the robot to adapt its behavior to facilitate efficient human-robot interaction in a variety of scenarios. Even in the absence of a human, additional sensor information can serve as a proxy for task success and current state. For instance, reactive preshaping techniques can be employed to modify a robot’s grip approach, preventing slipping, knocking objects over, or damaging delicate objects. Preshaping a grasp has been used with vision alone to correctly increase the success rate of picking up objects correctly [27]. Using touch for feedback during the grasp interaction resembles how humans use touch, sound, and vision to delicately interact with small or soft objects.

This survey examines state-of-the-art sensing methods for onboard close-proximity object detection near robot manipulators. It also explores how this information is processed and interpreted, with a particular focus on advancements made in improving human-robot interaction through real-time object avoidance. By investigating these advancements, we can gain insights into the integration of sensor data and its impact on enhancing the collaboration and interaction

between humans and robots.

## Chapter 2

### Onboard Sensors

#### 2.1 BioTac

The SynTouch BioTac sensor, depicted in fig. 2.1, is designed to mimic the human finger and incorporates three distinct sensor systems for detecting external stimuli [44]. At the tip of the BioTac sensor, there is a temperature sensor that is capable of detecting thermal flux in the vicinity of the fingertip. This sensor enables the sensor to perceive changes in temperature in its surrounding environment.

Another crucial feature of the BioTac sensor is an array of electrodes strategically placed throughout the area where a fingerprint is typically located. These electrodes are positioned beneath the outer elastomer layer and are separated from it by an incompressible conductive fluid, which is contained within a cavity. This configuration allows the BioTac sensor to capture detailed tactile information, similar to how human fingertips detect texture, shape, and other physical properties of objects. In addition to temperature and tactile sensing, the BioTac sensor incorporates a pressure sensor located in the rigid part of the finger near the mounting base. This pressure sensor detects the amount of force or pressure applied to the sensor, providing valuable information about the intensity of contact or interaction with external objects.

The BioTac sensor has been successfully used to achieve super-human vibration detection, particularly for practical applications such as object slip detection [16]. These vibrations are captured by the pressure sensor placed in the rigid body of the sensor. The conductive incompressible liquid layer carries the sound waves from the point of contact through a canal to the pressure

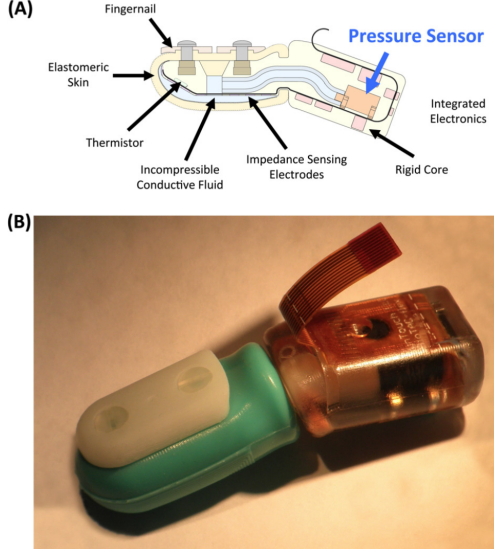


Figure 2.1: BioTac schematic and photo of the actual sensor are from [16].

sensor. The sensors ability to detect vibrations is primarily hindered by the presence of thermal amplification, which can interfere with the sensor's ability to accurately perceive and distinguish vibrations. Additionally, capacitively coupled extrinsic noise can impact the sensor's performance [16].

## 2.2 Optical-Tactile Sensors

Retrographic sensors employ an elastomeric layer covered by a reflective layer to determine object surface features by observing the deformation in the elastomer. A camera is positioned opposite to the contact point, with lights projecting red, green, and blue colors onto the surface. Through a photometric stereo algorithm, the object in contact with the surface is reconstructed [26]. One implementation of this concept is the GelSight sensor, designed specifically for robot grippers, as shown on the left side of fig. 2.2.

GelSight is a retrographic sensor that has been specifically developed for integration onto a robot end-effector. The GelSight sensor provides accurate contact surface reconstruction, force estimation, and slip detection capabilities [45, 9]. This sensor has been used to extract valuable

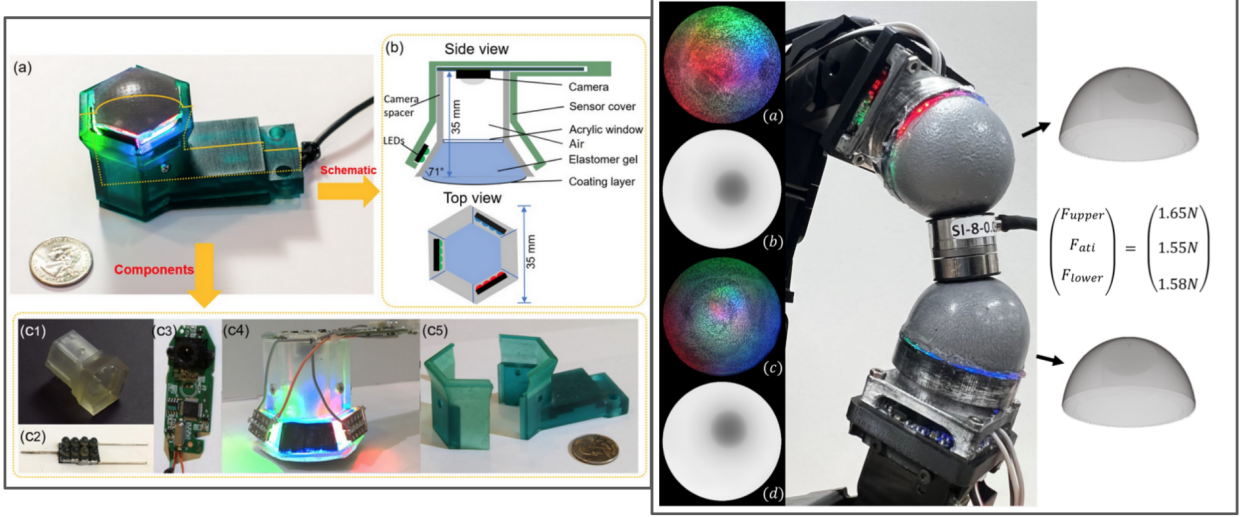


Figure 2.2: Two examples of optical-tactile sensors. The left image shows GelSight, from [9], and the right shows DenseTact 2.0, from [7].

information about liquid properties within a bottle through controlled robotic movements [25]. By analyzing time series data, GelSight enables the determination of liquid height and viscosity by assessing the principal motion of the liquid’s oscillations.

Expanding on the retrographic sensor concept, DenseTact introduces a half-sphere deformable elastomer layer, offering a wider field of view. This system generates point cloud depth estimates of objects in contact with the surface using a deep neural network trained on touch data from known shapes. The ground truth for training is derived from CAD models of the sensor and objects [8]. DenseTact 2.0 further enhances object shape reconstruction accuracy and incorporates a 6-axis wrench measurement for objects in contact, as depicted on the right side of fig. 2.2. Transfer learning is used to demonstrate the learned shape and force estimation algorithms on additional sensors [7].

While these optical-tactile sensors offer a pathway to accurate object interaction estimations, their current construction tends to be bulky. However, as the development of these gripper attachments progresses, it is anticipated that they will evolve towards a more finger-like form, resembling the human finger, rather than a planar or domed field of view.

### 2.3 Capacitive

Capacitive sensors offer the potential to detect human presence in an environment by measuring the capacitance coupling between a sensing surface and the human body. This sensing principle has been applied in a modular square form, allowing for the switching between tactile and proximity modes [21]. However, challenges arise when attempting to determine the applied force at high levels using this method. Building upon this, researchers have expanded the capabilities of capacitive sensing to include human hand tracking and interaction prediction. In a notable study, the authors successfully tracked the movements of two human hands simultaneously above the sensing surface [33]. The capacitive sensing array used in this work is depicted in the bottom left of Figure 2.3.

A sensing cuff was created to enhance robot manipulator collision avoidance by combining Time-of-Flight (ToF) and capacitive sensing [6]. ToF sensors encounter difficulties when detecting objects in close proximity, either due to limited sensing time or reflective material properties. To address these limitations, the sensing cuff integrates ToF and capacitive sensors, providing complementary proximity sensing capabilities. The cuff, depicted in the top of Figure 2.3, enables improved collision avoidance in robot manipulators.

A sensing surface with human-like compliance properties was developed by incorporating a grid of insulated conductive yarn between two silicon elastomers [40]. This design leverages mutual capacitance between the yarn layers to enable simultaneous detection of multiple contact locations. The resulting sensor, depicted in the bottom right of Figure 2.3, eliminates the need for an additional dielectric layer as the yarn provides electrical isolation. In addition to the sensor, the authors introduced a custom open-source PCB for signal processing and an imaging processing pipeline to visualize the applied forces.

### 2.4 Hexagonal Array

Rigid hexagonal printed circuit boards (PCBs) have been introduced to cover entire robot bodies, incorporating multiple sensing modalities [32, 2]. These sensor units offer acceleration,

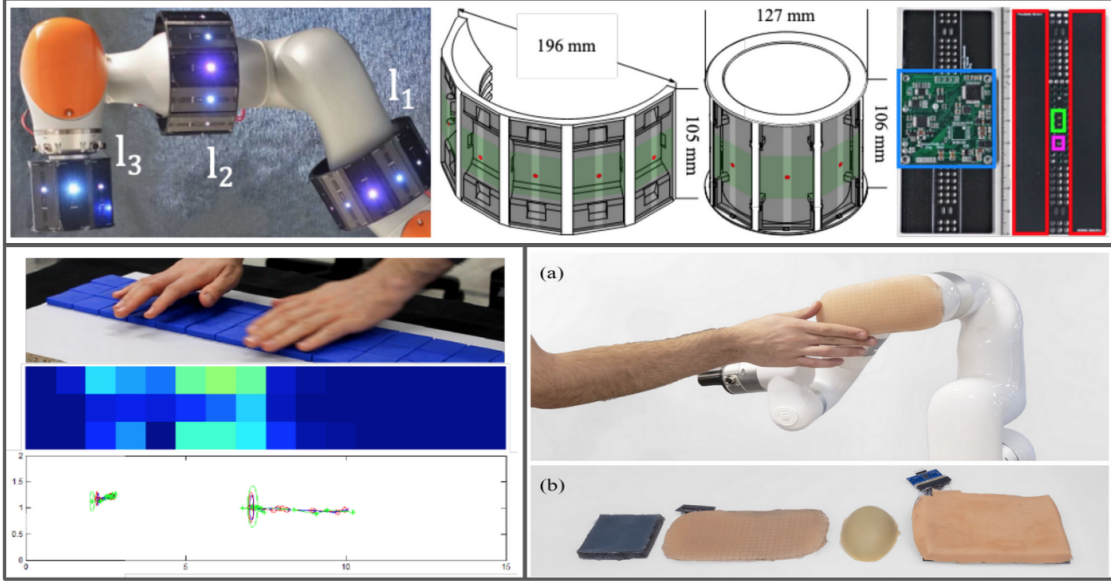


Figure 2.3: Sensors that incorporate capacitive sensing as one of their sensing modalities. Top uses time-of-flight and capacitive sensing, from [6]. Bottom left image shows a capacitive sensing array ,from [33], providing both proximity and tactile information. The bottom right image uses a mutual capacitance grid to preform multi-touch localization on human-like skin [40].

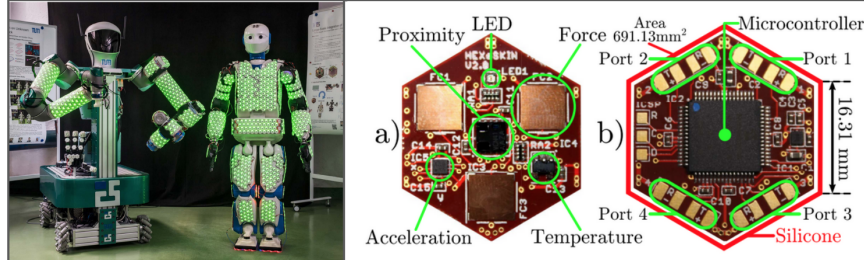


Figure 2.4: Left shows robots equipped with an array of hexagonal sensor units to cover the entire robot. Right shows breakdown of single sensor unit. Both from [2].

proximity, force, and temperature sensing capabilities, along with a microcontroller and four ports for connecting other sensors. The sensors are strategically placed on robot bodies and feet, as depicted in Figure 2.4, which provides a zoomed-in view of the sensor unit. One notable contribution of these works is the formalization of the connection method between multiple sensors, reducing the burden of wiring. The integrated design of these sensors enables their placement on the feet of humanoid robots, showcasing their durability.

## 2.5 Acoustic

Piezoelectric transducers are employed to transform the entire surface of a robot into a proximity sensor by examining the interference patterns caused by external objects [15]. In this setup, one piezoelectric transducer transmits an acoustic frequency, while another placed at the opposite end of the link receives it. This sensing principle and an example setup are illustrated at the top of Figure 2.5. Piezoelectric transducers are used as an additional sensing modality to enable whole-surface contact location and force prediction for single-point contact on a robot arm [14]. Location and force estimation are achieved by training a support vector machine on specific frequencies, emphasizing high touch sensitivity and low sensitivity to external noise. Multiple everyday objects are employed to demonstrate the system's sensitivity to unique physical characteristics in both proximity and contact evaluation scenarios.

In order to detect contact along a soft pneumatic finger, a microphone and a speaker were embedded within the finger's air chamber, as depicted at the bottom of Figure 2.5 [46]. The finger emits a frequency sweep that is captured by the microphone. Subsequently, a k-nearest neighbors algorithm is employed to distinguish touch locations along the finger based on the audio data. These sensors demonstrate sufficient sensitivity to function as a 2-D array of tactile sensors along the soft finger. This capability was leveraged in an example application where the sensors were used to read Braille [41].

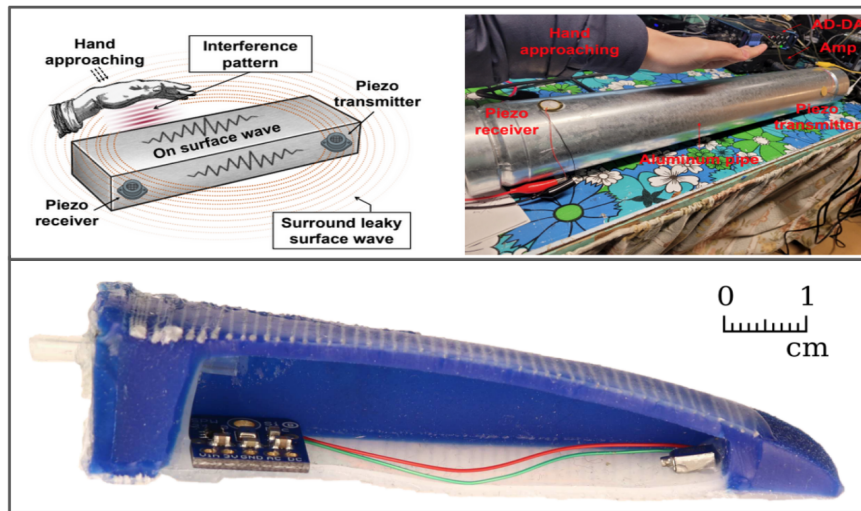


Figure 2.5: Bottom finger-like sensor with speaker and microphone, from [46]. Top shows the acoustic proximity detection principle on the left and an example setup with two piezos on the right, from [15].

## Chapter 3

### Control with Sensing Feedback

All of the papers discussed in this section use sensor information to dynamically adjust the behavior of robot manipulators in real-time. Unlike other sensor-related research chapter 2, where sensors are often external to the robot, the sensors in these papers are placed directly on the robot body or end-effector. The goal is to improve safety and enhance the robot's ability to complete tasks effectively. One approach involves incorporating proprioceptive feedback at the joints using force/torque sensors. Using these sensors and the robot's dynamics model, the robot can detect contact and determine the direction of the contact, enabling reactive behavior without the need for external sensors [3]. To further enhance collision detection and avoidance capabilities, researchers have developed a collision detection pipeline, as depicted at the bottom of Figure 3.1. This pipeline analyzes various control and detection methods, considering the advantages and disadvantages of each approach. Special attention is given to limiting the energy generated during a collision to minimize damage in human-robot interaction scenarios [22].

In order to prevent collisions, certain methods employ a safety margin around the robot, wherein robot movement is halted if an object enters this zone. One example is the use of piezoelectric sensors to create a proximity field around a robot arm, enabling the detection of objects and subsequent stopping of arm movement to avoid collisions [15]. Although this approach does not provide detailed information about the potential collision, it serves as a cost-effective method to prevent contact. The detection and movement stop pipeline for this method is depicted on the left side of Figure 3.2. To further reduce the impact force during contact with a robot manipulator,

an adjustable stiffness impedance controller was proposed in [5]. This approach uses proximity information from sensing cuffs (as detailed in Chapter 2) to adjust the stiffness of the robot manipulator. When an object is in close proximity, the stiffness is reduced to minimize the force exerted. While in the absence of nearby objects, the stiffness is increased to improve the precision of the robot manipulator's movements. A visual representation of this behavior is presented on the right side of Figure 3.2.

In order to provide an iCub robot with a sense of peripersonal space, a combination of vision and tactile sensors was utilized. Peripersonal space refers to the space near the robot where objects can be manipulated and interactions may take place. The iCub robot, depicted at the top of Figure 3.3, learns to perceive the probability of contact with specific taxels along its body through visual observations, self-touch experiences, and interactions with external objects [38]. This information is then used to attract or repel the point closest to the detected contact location, enabling the robot

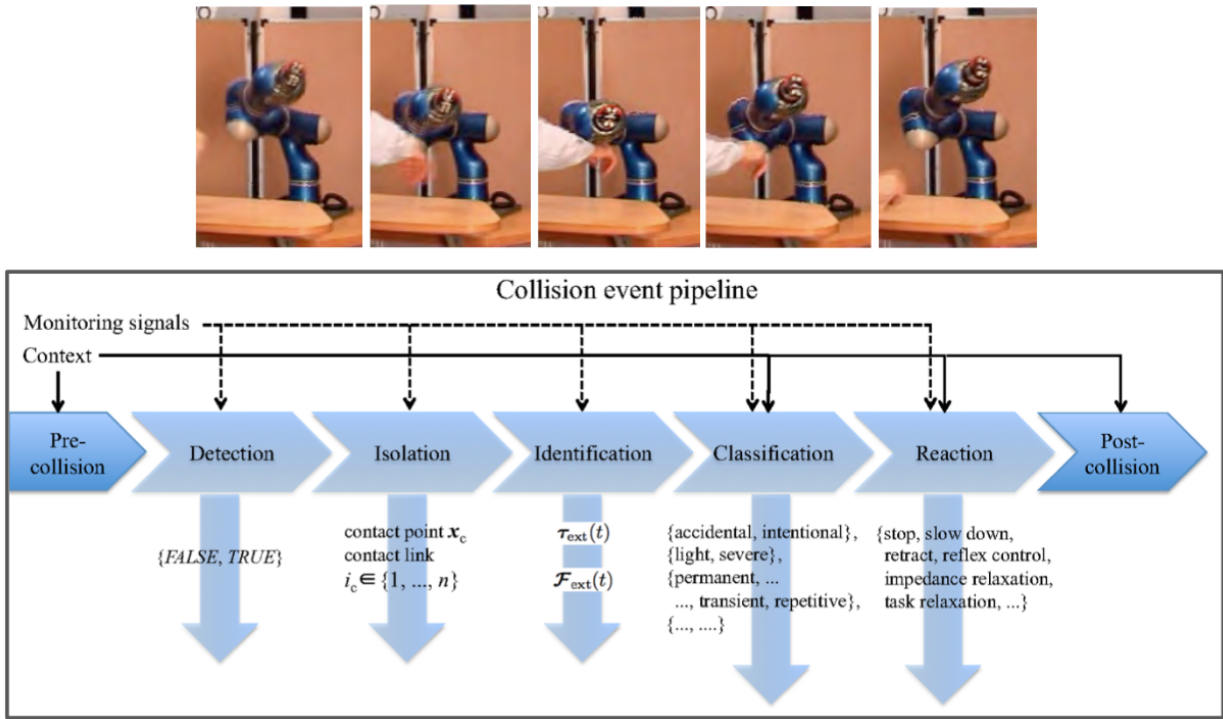


Figure 3.1: Top shows an example human collision detection using only proprioceptive sensors, adapted from [3]. Bottom shows a seven event collision detection pipeline, presented in [22].

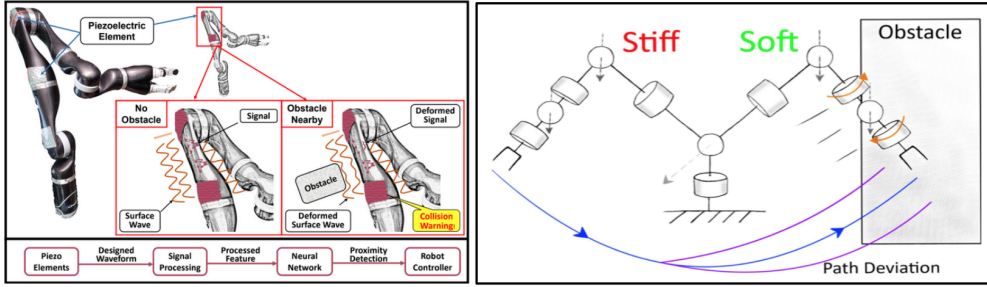


Figure 3.2: Left shows the proximity signal detection and robot stopping pipeline from [15]. Right shows stiffness adjustment and path deviation to reduce collision force ,from [5].

to interact with objects in its peripersonal space.

A comprehensive survey, conducted by [34], examines the applications and methods for robots equipped with proximity sensors. The survey categorizes the applications into two main categories: sensors integrated within the robot gripper and sensors distributed throughout the robot's body. Sensors integrated with the gripper enable robots to adjust their grasp and make informed decisions before making contact with an object, as demonstrated in the bottom of Figure 3.3. In contrast, body sensors are primarily used to ensure safety during human-robot interactions. Both systems contribute to improving the robot's perception of its immediate surroundings. The survey also discusses various proximity sensing methods commonly employed, such as optical and capacitive principles.

Robots equipped with a capacitive sensing array at the end-effector, as depicted in the top of Figure 3.4, have been successfully used in real-world scenarios involving human subjects, such as dressing and washing tasks [13]. The capacitive array provides valuable information through cloth surfaces, enabling accurate estimation of the position of a human arm or leg. This capability is particularly useful when vision systems cannot accurately estimate limb positions when they are out of sight. In the implementation described, a neural network is trained to predict the end-effector location relative to the limb, and a control algorithm estimates the direction in which the robot should move to follow a path along the arm. This allows the robot to apply appropriate pressure during washing or hover above the limb during dressing, as demonstrated in the respective

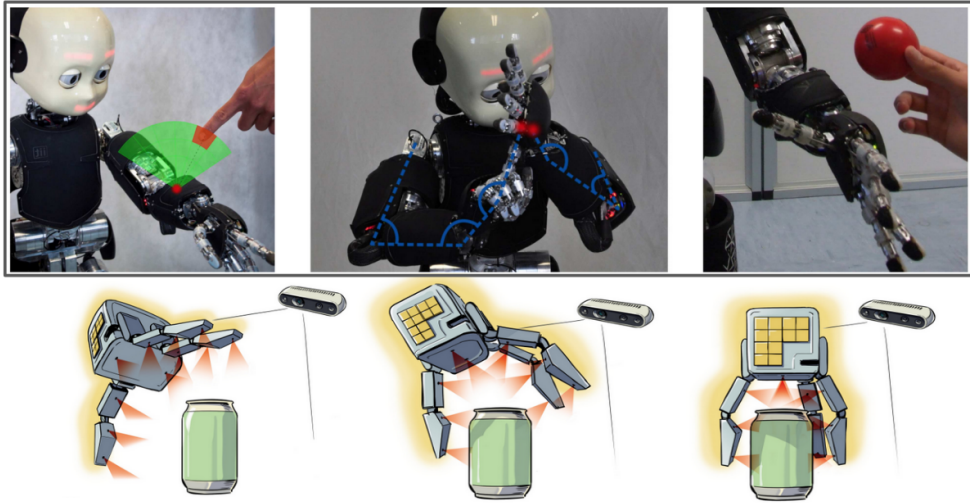


Figure 3.3: Top shows the iCub robot with taxel sensors along its body. These are used along with its vision system to estimate where objects near the body are most likely to make contact [38]. Bottom shows an adapted visual reactive preshaping example using proximity sensors for the robot gripper to adjust a grab approach prior to making contact [34].

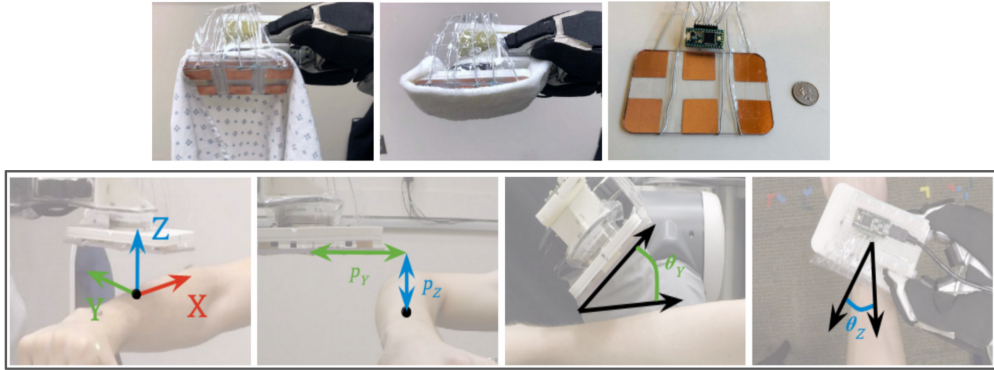


Figure 3.4: Top shows capacitive sensor array used for autonomous human dressing and washing tasks. Bottom shows the coordinate axes and variables used to formally define the end-effector position relative to a human limb. Images adapted from [13].

scenarios. The bottom of Figure 3.4 provides a visualization of the coordinate axes and variables utilized to estimate the end-effector position relative to the limb.

## **Chapter 4**

### **Control**

In this chapter, our focus is on robot arm control strategies that aim to achieve collision avoidance while also considering additional secondary objectives. The key aspect we explore is how each method harnesses sensor information to determine the appropriate movement of the robot arm.

In the context of robot arm control for collision avoidance, a human-robot collision avoidance algorithm was proposed in [18]. This algorithm utilizes depth information obtained from an externally mounted sensor to detect objects in close proximity to the robot manipulator. To handle occluded spaces where an object obstructs the camera's view, the algorithm projects the object back as a line in space. The closest point on this line to the robot is considered as the object location, as illustrated in the top left of Figure 4.1. From these object locations, repulsive vectors are computed and applied to the robot end-effector based on the object's velocity. If the object's velocity is known, the repulsive vector is adjusted to be orthogonal to the object's velocity direction, rather than simply moving directly away from the current object position. The repulsive velocities are depicted in the bottom left of Figure 4.1, along with a real-world collision avoidance example shown on the right. To avoid collisions with objects, the robot body converts Cartesian constraints to joint velocity constraints. This limits the movement of body control points towards objects, allowing the robot to use its redundant degrees of freedom while ensuring primary avoidance of the end-effector [17].

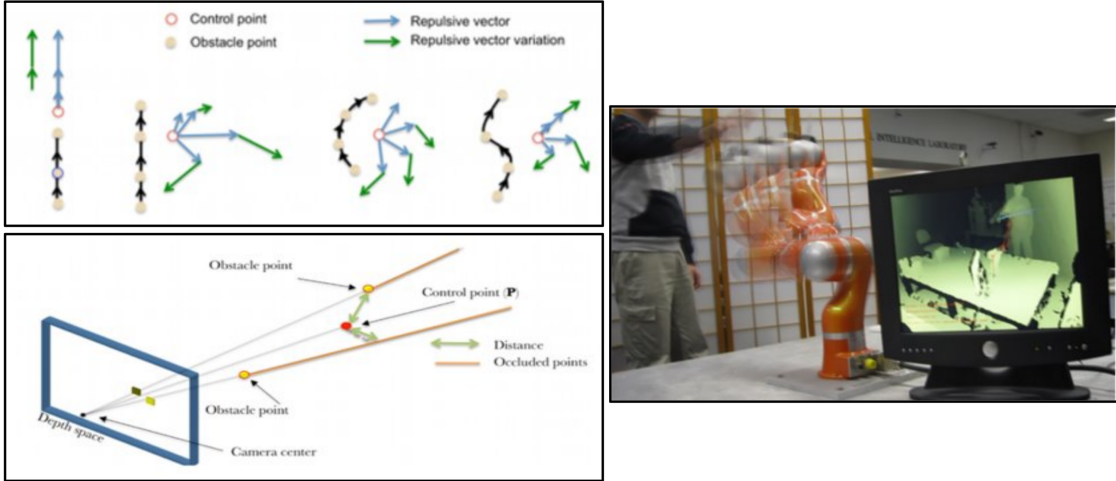


Figure 4.1: Top left shows the repulsive vectors to a control point, such as the end-effector, when the object velocity is included or excluded. Bottom left shows how object distances are calculated with occlusions from the camera’s point of view. Right shows the raw depth data on the screen while a human approaches the robot, triggering avoidance behavior. Figures are from [18].

## 4.1 Quadratic Programming Optimization

All of the methods discussed in this chapter employ a quadratic programming (QP) formulation to optimize the robot end-effector velocity, taking into account multiple constraints to achieve collision avoidance while maintaining the desired trajectory.

In the QP formulation presented in [4], shown in the bottom left of fig. 4.2, the objective function consists of two terms: 1) the desired robot end-effector velocity and 2) singularity avoidance. The constraints related to object avoidance, except for joint limits, are expressed in the linear inequality constraint vector  $\mathbf{b}$ . The severity of the avoidance behavior is determined by a hand-tuned distance function that incorporates a minimum avoidance distance, as depicted in fig. 4.2. To avoid local minima configurations, an additional term is added to the inequality constraint vector, increasing the overall distance to all objects. It has been demonstrated that this collision avoidance method works effectively when using custom-built sensors chapter 2.

An alternative QP method for robot arm control is presented in [23], which incorporates manipulability as an additional objective function to optimize. The manipulability ellipsoids, rep-

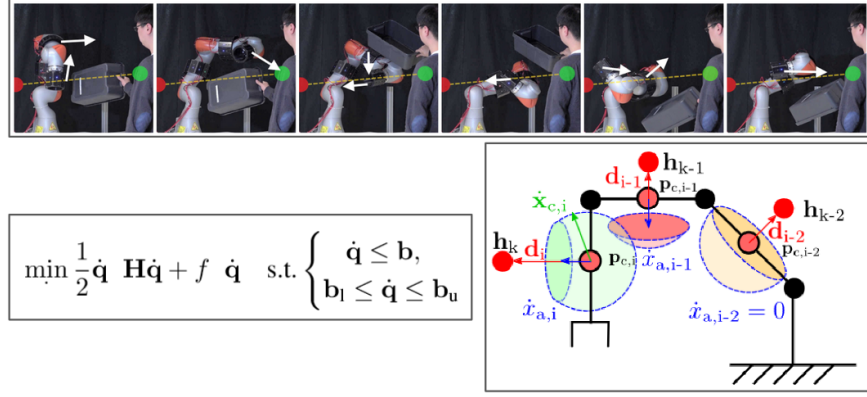


Figure 4.2: Top shows obstacle avoidance while the robot end-effector moves between two points. Bottom left shows a common quadratic programming formulation for objective functions with constraints. Bottom right illustrates how movement restrictions are placed along the robot body for multiple objects. The colored spheres are the acceptable velocities for each of the points that can move. Figures are from [4].

resenting the translational and angular capabilities of the robot end-effector, indicate the ability of the robot arm to generate different velocities. An example showcasing two robot configurations with different angular velocity capabilities is shown in the top of fig. 4.3. The authors formulate a manipulability Jacobian that relates joint velocities to changes in the manipulability measure. They also address joint limits by employing a velocity dampening method, which adjusts the velocities based on the proximity of each joint to its limits. Building upon this work, [24] introduces obstacle avoidance constraints while maximizing manipulability. They extend the velocity dampening technique to consider the distance between nearby objects and an arbitrary point along the manipulator. By incorporating these additional terms, the end-effector can avoid both static and dynamic objects by deviating from the specified task, as depicted in the bottom right of fig. 4.3. To prevent local minima, a retracting function is implemented, moving away from the object to explore new angles of approach.

#### 4.1.1 Explicit Reference Governor

The method presented in [31] focuses on controlling a robot arm and avoiding obstacles using a dynamic model of the manipulator. It ensures smooth constrained motion through two

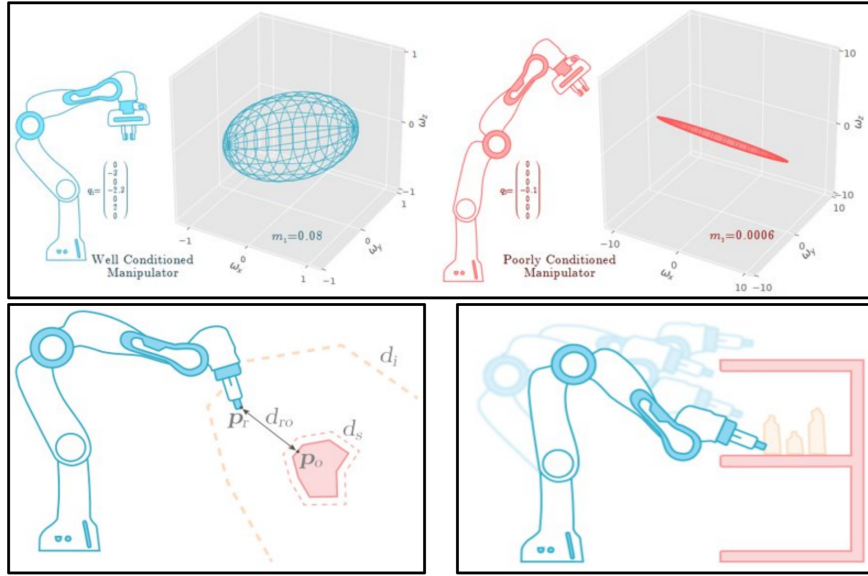


Figure 4.3: Top image shows the robot end-effector’s angular velocity manipulability ellipsoid in two configurations, from [23]. Bottom left image shows the object avoidance calculation distance with a minimum avoidance distance around the object. Bottom right shows an example scenario where a robot avoids a collision and achieves a goal position. Bottom images are from [24].

steps. First, a trajectory-based explicit reference governor is employed, which uses a navigation field and a dynamic safety margin to impose joint restrictions based on the robot’s dynamics. The dynamic safety margin uses the robots dynamics to predict the forward dynamics and joint limits from a set time simulation using simplistic euler, shown in the bottom left of fig. 4.4. Second, a pre-stabilized PD and gravity control system is used to send velocities to the robot. This allows the robot to achieve the desired motion while considering the constraints imposed by the reference governor. One notable advantage of this method is that it does not require online optimization to be solved, setting it apart from other approaches discussed in this document. Objects in the environment are modeled as geometric primitives, enabling efficient distance calculations. In static environments, this method provides a guarantee of constraint satisfaction and asymptotic stability with respect to the navigational field. The robot’s joints will reach their goal configurations given enough time. The paper demonstrates a real-world dynamic avoidance experiment using vicon tracking markers to measure obstacle distances. The resulting robot movement exhibits different

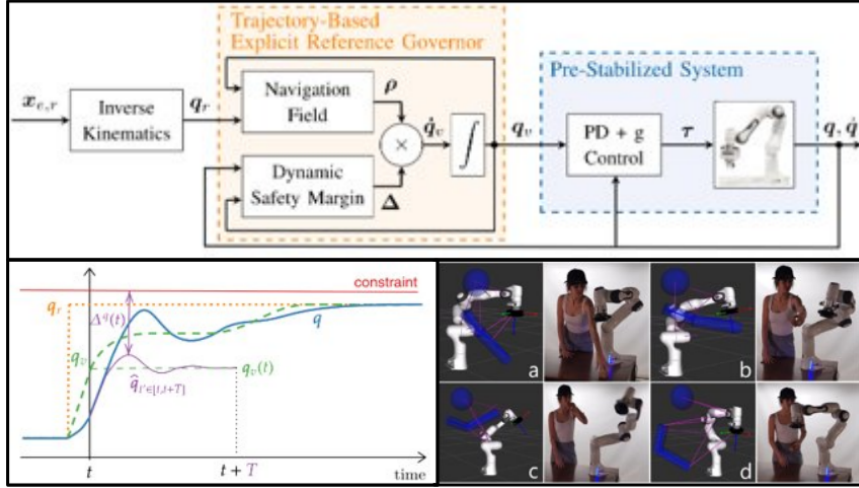


Figure 4.4: Top diagram shows the control blocks for the ERG based collision avoidance controller. Bottom left shows an example dynamic safety margin prediction and actual joint positions over time. Bottom right shows a real-world avoidance example using vicon markers for sensing the human subject. All figures are from [31].

characteristics compared to other avoidance methods. Further investigation can be conducted to assess user preferences, maximum speed, and the perceived quality of the avoidance motion in comparison to alternative approaches.

## 4.2 Non-Linear Optimization

A weighted-sum non-linear constrained optimization formulation was proposed in [36] to solve for the inverse kinematics of a robot manipulator with multiple objective functions. Each objective function is normalized and combined using a Gaussian surrounded by a polynomial, as illustrated in Figure 4.5. Additionally, object collision avoidance is incorporated as an additional objective term, where the three closest object distances are considered for avoidance behavior. To handle objects that enter and exit a predefined threshold during avoidance, objects near the robot are represented as convex hulls. Point cloud data is converted to a convex hull representation when a geometric primitive such as a sphere or rectangle is not predetermined in the scene, as depicted in Figure 4.6. This approach allows for adaptability in handling different types of objects and obstacle avoidance. To accommodate multiple types of objective functions with unique goal criteria, three

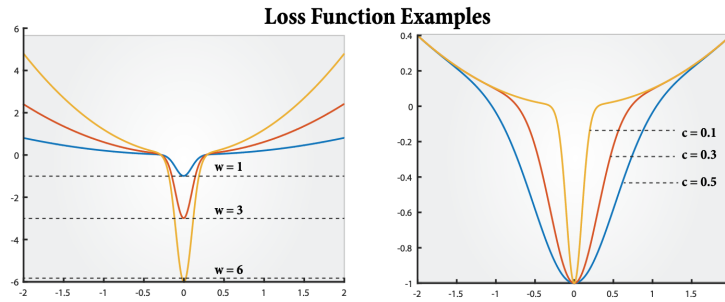


Figure 4.5: Objective normalization function of a gaussian surrounded by a polynomial, from [36].

task categories with specifically shaped barrier method loss functions have been introduced in [43]. Examples of these task categories and their corresponding loss functions are shown in Figure 4.7. These methods enable robots to adhere to multiple goals simultaneously. However, it is important to note that there may be instances where the objectives compete with one another or result in ill-conceived behavior. Therefore, dynamic alteration of these loss functions could be considered based on the context of a particular interaction.

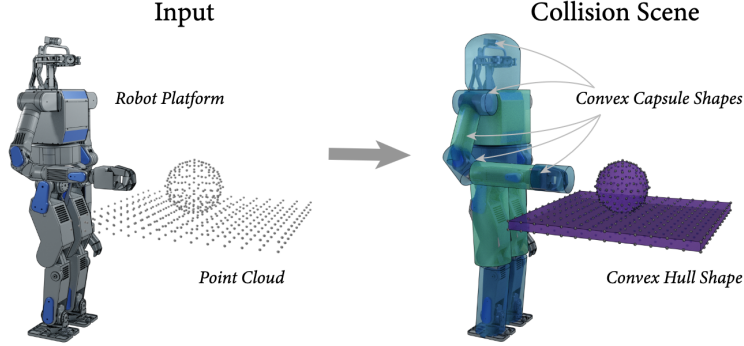


Figure 4.6: Point cloud to convex hull representation for collision avoidance objective functions [37].

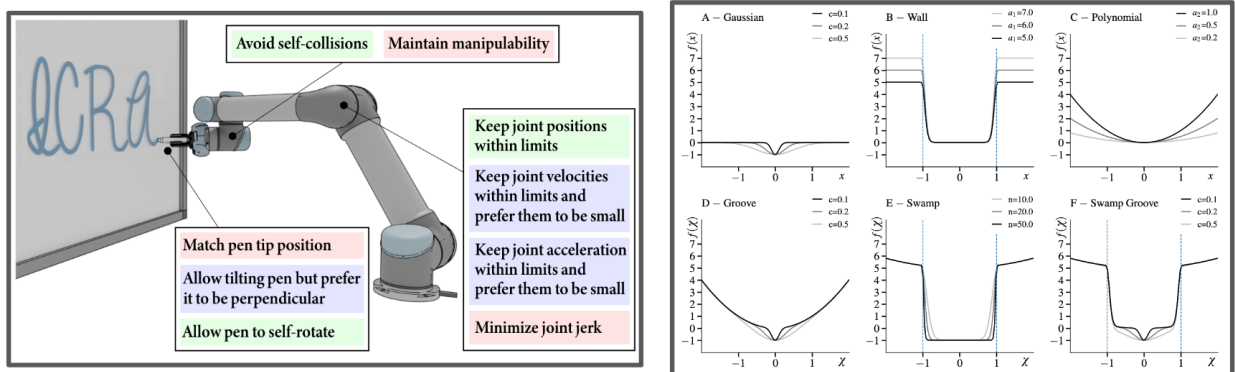


Figure 4.7: The left image shows example robot arm objective function types: Red – specific goal, Green – range of equally valid goals, and Blue – range of goal with a preference toward certain values. These correspond to the Groove, Swamp, and Swamp Groove graphs, respectively. These figures were adapted from [43].

## **Chapter 5**

### **Conclusions**

This document provides a summary of the existing research at the intersection of sensing systems and robot arm motion control for real-time collision avoidance. It emphasizes the importance of integrating sensors with robot grippers and bodies to enhance safety and manipulation during interactions with human collaborators. While there are numerous sensing methods available, the full potential of sensor information is still underutilized. Recent publications have explored using existing sensors to detect specific material properties, capture dynamic motion, improve workspace estimations, and modify sensor form factors. For instance, the GelSight paper [45], published in 2017, has garnered significant attention, with subsequent works exploring alternative sensor shapes [28, 42, 35, 1, 39]. However, equipping a robot arm with onboard sensors remains a costly, time-consuming, and challenging task. Most collaborative robot (CoBot) systems are equipped with internal force/torque sensors to meet minimum collision detection requirements set by standards such as ISO [19]. While some robotics companies offer robots with built-in sensors, such as NEURA Robotics and Boston Dynamics, the add-on options are typically limited to vision, depth, force, and auditory systems [20, 11]. With the growing integration of onboard sensors in robots and the increasing availability of sensing systems that are easy to integrate and cost-effective, research in robot interaction systems will harness sensor data to further enhance collaboration between humans and robots. Sensor information can be used to adjust trajectories, prioritizing legibility and predictability for human users, leading to improved user interactions [10]. A review on tactile information has categorized the types of data that tactile sensors can provide, such as local geometry,

forces and torques, contact events, and material properties. The review also includes a compilation of papers that leverage tactile information for informed robot control [30].

Robots have transitioned from their traditional caged industrial workspaces to operating in close proximity to humans, relying on perception systems to avoid harm. While commercially available robots with integrated sensors and feedback control methods are not yet widespread, ongoing research suggests that it will become increasingly common for robots to integrate multiple onboard data streams to perform tasks at a level comparable to or surpassing human capabilities.

## Bibliography

- [1] Alex Alspach, Kuniyatsu Hashimoto, Naveen Kuppuswamy, and Russ Tedrake. Soft-bubble: A highly compliant dense geometry tactile sensor for robot manipulation. In 2019 2nd IEEE International Conference on Soft Robotics (RoboSoft), pages 597–604. IEEE, 2019.
- [2] Gordon Cheng, Emmanuel Dean-Leon, Florian Bergner, Julio Rogelio Guadarrama Olvera, Quentin Leboutet, and Philipp Mittendorfer. A comprehensive realization of robot skin: Sensors, sensing, control, and applications. Proceedings of the IEEE, 107(10):2034–2051, 2019.
- [3] Alessandro De Luca, Alin Albu-Schaffer, Sami Haddadin, and Gerd Hirzinger. Collision detection and safe reaction with the dlr-iii lightweight manipulator arm. In 2006 IEEE/RSJ International Conference on Intelligent Robots and Systems, pages 1623–1630. IEEE, 2006.
- [4] Yitao Ding and Ulrike Thomas. Collision avoidance with proximity servoing for redundant serial robot manipulators. In 2020 IEEE International Conference on Robotics and Automation (ICRA), pages 10249–10255. IEEE, 2020.
- [5] Yitao Ding and Ulrike Thomas. Improving safety and accuracy of impedance controlled robot manipulators with proximity perception and proactive impact reactions. In 2021 IEEE International Conference on Robotics and Automation (ICRA), pages 3816–3821. IEEE, 2021.
- [6] Yitao Ding, Felix Wilhelm, Leonhard Faulhammer, and Ulrike Thomas. With proximity servoing towards safe human-robot-interaction. In 2019 IEEE/RSJ International Conference on Intelligent Robots and Systems (IROS), pages 4907–4912. IEEE, 2019.
- [7] Won Kyung Do, Bianca Jurewicz, and Monroe Kennedy III. Densetact 2.0: Optical tactile sensor for shape and force reconstruction. arXiv preprint arXiv:2209.10122, 2022.
- [8] Won Kyung Do and Monroe Kennedy. Densetact: Optical tactile sensor for dense shape reconstruction. In 2022 International Conference on Robotics and Automation (ICRA), pages 6188–6194. IEEE, 2022.
- [9] Siyuan Dong, Wenzhen Yuan, and Edward H Adelson. Improved gelsight tactile sensor for measuring geometry and slip. In 2017 IEEE/RSJ International Conference on Intelligent Robots and Systems (IROS), pages 137–144. IEEE, 2017.
- [10] Anca D Dragan, Kenton CT Lee, and Siddhartha S Srinivasa. Legibility and predictability of robot motion. In 2013 8th ACM/IEEE International Conference on Human-Robot Interaction (HRI), pages 301–308. IEEE, 2013.

- [11] Boston Dynamics. Boston Dynamics main website landing, 1992.
- [12] John Ennin. TE Connectivity sensors for the connected car, 2016.
- [13] Zackory Erickson, Henry M Clever, Vamsee Gangaram, Greg Turk, C Karen Liu, and Charles C Kemp. Multidimensional capacitive sensing for robot-assisted dressing and bathing. In 2019 IEEE 16th International Conference on Rehabilitation Robotics (ICORR), pages 224–231. IEEE, 2019.
- [14] Xiaoran Fan, Daewon Lee, Larry Jackel, Richard Howard, Daniel Lee, and Volkan Isler. Enabling low-cost full surface tactile skin for human robot interaction. IEEE Robotics and Automation Letters, 7(2):1800–1807, 2022.
- [15] Xiaoran Fan, Riley Simmons-Edler, Daewon Lee, Larry Jackel, Richard Howard, and Daniel Lee. Aurasense: Robot collision avoidance by full surface proximity detection. In 2021 IEEE/RSJ International Conference on Intelligent Robots and Systems (IROS), pages 1763–1770. IEEE, 2021.
- [16] Jeremy A Fishel and Gerald E Loeb. Sensing tactile microvibrations with the bio-tac—comparison with human sensitivity. In 2012 4th IEEE RAS & EMBS international conference on biomedical robotics and biomechatronics (BioRob), pages 1122–1127. IEEE, 2012.
- [17] Fabrizio Flacco, Alessandro De Luca, and Oussama Khatib. Motion control of redundant robots under joint constraints: Saturation in the null space. In 2012 IEEE International Conference on Robotics and Automation, pages 285–292. IEEE, 2012.
- [18] Fabrizio Flacco, Torsten Kröger, Alessandro De Luca, and Oussama Khatib. A depth space approach to human-robot collision avoidance. In 2012 IEEE international conference on robotics and automation, pages 338–345. IEEE, 2012.
- [19] International Organization for Standardization. International Organization for Standardization robots and robotic devices — safety requirements for industrial robots — part 1: Robots, 2011.
- [20] NEURA Robotics GmbH. NEURA Robotics main website landing, 2019.
- [21] Dirk Göger, Hosam Alagi, and Heinz Wörn. Tactile proximity sensors for robotic applications. In 2013 IEEE International Conference on Industrial Technology (ICIT), pages 978–983. IEEE, 2013.
- [22] Sami Haddadin, Alessandro De Luca, and Alin Albu-Schäffer. Robot collisions: A survey on detection, isolation, and identification. IEEE Transactions on Robotics, 33(6):1292–1312, 2017.
- [23] Jesse Haviland and Peter Corke. A purely-reactive manipulability-maximising motion controller. arXiv preprint arXiv:2002.11901, 2020.
- [24] Jesse Haviland and Peter Corke. Neo: A novel expeditious optimisation algorithm for reactive motion control of manipulators. IEEE Robotics and Automation Letters, 6(2):1043–1050, 2021.

- [25] Hung-Jui Huang, Xiaofeng Guo, and Wenzhen Yuan. Understanding dynamic tactile sensing for liquid property estimation. *arXiv preprint arXiv:2205.08771*, 2022.
- [26] Micah K Johnson and Edward H Adelson. Retrographic sensing for the measurement of surface texture and shape. In *2009 IEEE Conference on Computer Vision and Pattern Recognition*, pages 1070–1077. IEEE, 2009.
- [27] Oliver B Kroemer, Renaud Detry, Justus Piater, and Jan Peters. Combining active learning and reactive control for robot grasping. *Robotics and Autonomous systems*, 58(9):1105–1116, 2010.
- [28] Mike Lambeta, Po-Wei Chou, Stephen Tian, Brian Yang, Benjamin Maloon, Victoria Rose Most, Dave Stroud, Raymond Santos, Ahmad Byagowi, Gregg Kammerer, et al. Digit: A novel design for a low-cost compact high-resolution tactile sensor with application to in-hand manipulation. *IEEE Robotics and Automation Letters*, 5(3):3838–3845, 2020.
- [29] Matt Leonard. Supply Chain Dive declining price of iot sensors means greater use in manufacturing, 2019.
- [30] Qiang Li, Oliver Kroemer, Zhe Su, Filipe Fernandes Veiga, Mohsen Kaboli, and Helge Joachim Ritter. A review of tactile information: Perception and action through touch. *IEEE Transactions on Robotics*, 36(6):1619–1634, 2020.
- [31] Kelly Merckaert, Bryan Convens, Chi-ju Wu, Alessandro Roncone, Marco M Nicotra, and Bram Vanderborght. Real-time motion control of robotic manipulators for safe human–robot coexistence. *Robotics and Computer-Integrated Manufacturing*, 73:102223, 2022.
- [32] Philipp Mittendorfer and Gordon Cheng. Uniform cellular design of artificial robotic skin. In *ROBOTIK 2012; 7th German Conference on Robotics*, pages 1–5. VDE, 2012.
- [33] Stefan Escaida Navarro, Maximiliano Marufo, Yitao Ding, Stephan Puls, Dirk Göger, Björn Hein, and Heinz Wörn. Methods for safe human-robot-interaction using capacitive tactile proximity sensors. In *2013 IEEE/RSJ International Conference on Intelligent Robots and Systems*, pages 1149–1154. IEEE, 2013.
- [34] Stefan Escaida Navarro, Stephan Mühlbacher-Karrer, Hosam Alagi, Hubert Zangl, Keisuke Koyama, Björn Hein, Christian Duriez, and Joshua R Smith. Proximity perception in human-centered robotics: A survey on sensing systems and applications. *IEEE Transactions on Robotics*, 38(3):1599–1620, 2021.
- [35] Akhil Padmanabha, Frederik Ebert, Stephen Tian, Roberto Calandra, Chelsea Finn, and Sergey Levine. Omnitact: A multi-directional high-resolution touch sensor. In *2020 IEEE International Conference on Robotics and Automation (ICRA)*, pages 618–624. IEEE, 2020.
- [36] Daniel Rakita, Bilge Mutlu, and Michael Gleicher. Relaxeddik: Real-time synthesis of accurate and feasible robot arm motion. In *Robotics: Science and Systems*, pages 26–30. Pittsburgh, PA, 2018.
- [37] Daniel Rakita, Haochen Shi, Bilge Mutlu, and Michael Gleicher. Collisionik: A per-instant pose optimization method for generating robot motions with environment collision avoidance. In *2021 IEEE International Conference on Robotics and Automation (ICRA)*, pages 9995–10001. IEEE, 2021.

- [38] Alessandro Roncone, Matej Hoffmann, Ugo Pattacini, Luciano Fadiga, and Giorgio Metta. Peripersonal space and margin of safety around the body: learning visuo-tactile associations in a humanoid robot with artificial skin. *PloS one*, 11(10):e0163713, 2016.
- [39] Huanbo Sun, Katherine J Kuchenbecker, and Georg Martius. A soft thumb-sized vision-based sensor with accurate all-round force perception. *Nature Machine Intelligence*, 4(2):135–145, 2022.
- [40] Marc Teyssier, Brice Parilusyan, Anne Roudaut, and Jürgen Steimle. Human-like artificial skin sensor for physical human-robot interaction. In 2021 IEEE International Conference on Robotics and Automation (ICRA), pages 3626–3633. IEEE, 2021.
- [41] Vincent Wall and Oliver Brock. A virtual 2d tactile array for soft actuators using acoustic sensing. In 2022 IEEE/RSJ International Conference on Intelligent Robots and Systems (IROS), pages 10029–10034. IEEE, 2022.
- [42] Shaoxiong Wang, Yu She, Branden Romero, and Edward Adelson. Gelsight wedge: Measuring high-resolution 3d contact geometry with a compact robot finger. In 2021 IEEE International Conference on Robotics and Automation (ICRA), pages 6468–6475. IEEE, 2021.
- [43] Yeping Wang, Pragathi Praveena, Daniel Rakita, and Michael Gleicher. Rangedik: An optimization-based robot motion generation method for ranged-goal tasks. arXiv preprint arXiv:2302.13935, 2023.
- [44] Nicholas Wettels, Veronica J Santos, Roland S Johansson, and Gerald E Loeb. Biomimetic tactile sensor array. *Advanced robotics*, 22(8):829–849, 2008.
- [45] Wenzhen Yuan, Siyuan Dong, and Edward H Adelson. Gelsight: High-resolution robot tactile sensors for estimating geometry and force. *Sensors*, 17(12):2762, 2017.
- [46] Gabriel Zöller, Vincent Wall, and Oliver Brock. Active acoustic contact sensing for soft pneumatic actuators. In 2020 IEEE International Conference on Robotics and Automation (ICRA), pages 7966–7972. IEEE, 2020.